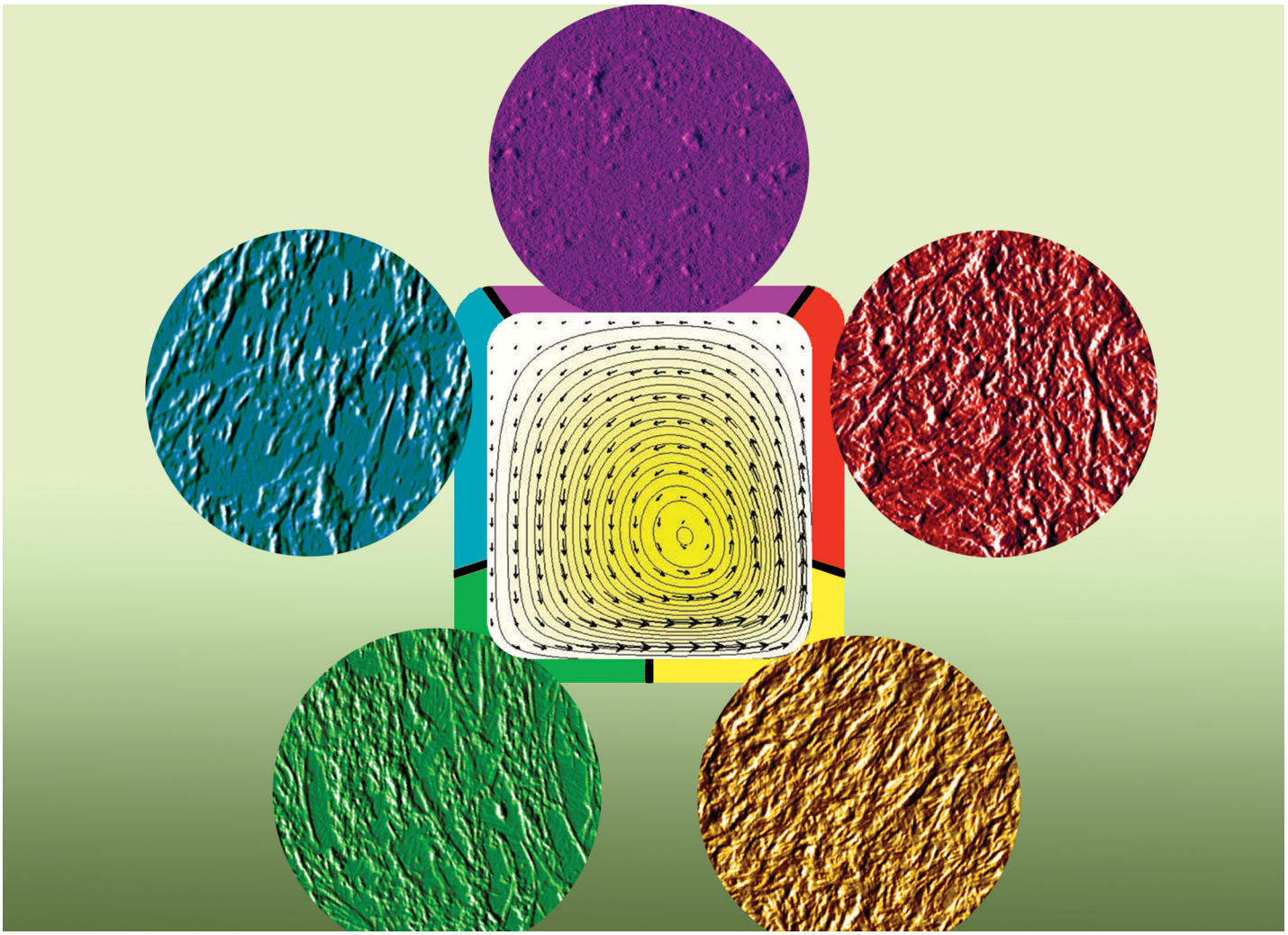

Highlighting research results from Rensselaer Polytechnic Institute, Troy, NY, and Arizona State University, Tempe, AZ; USA.

Surface shear viscosity as a macroscopic probe of amyloid fibril formation at a fluid interface

Formation of amyloid fibrils on the surface of a protein solution being sheared was studied through proteomic techniques along with experimental and computational fluid dynamics. The rapid growth of the fibril weave observed at the surface was found to be associated with the momentum boundary layer just beneath it.

As featured in:

See Amir H. Hirsa *et al.*, *Soft Matter*, 2017, **13**, 1780.

ROYAL SOCIETY OF CHEMISTRY

rsc.li/soft-matter-journal

Registered charity number: 207890

Soft Matter

PAPER

Cite this: *Soft Matter*, 2017, **13**, 1780

Surface shear viscosity as a macroscopic probe of amyloid fibril formation at a fluid interface

Vignesh S. Balaraj,[a] Philip C. H. Zeng,[ab] Sean P. Sanford,[b] Samantha A. McBride,[c] Aditya Raghunandan,[a] Juan M. Lopez[d] and Amir H. Hirsa*[ac]

Received 9th August 2016,
Accepted 29th January 2017

DOI: 10.1039/c6sm01831a

rsc.li/soft-matter-journal

Amyloidogenesis of proteins is of wide interest because amyloid structures are associated with many diseases, including Alzheimer's and type II diabetes. Dozens of different proteins of various sizes are known to form amyloid fibrils. While there are numerous studies on the fibrillization of insulin induced by various perturbations, shearing at fluid interfaces has not received as much attention. Here, we present a study of human insulin fibrillization at room temperature using a deep-channel surface viscometer. The hydrodynamics of the bulk flow equilibrates in just over a minute, but the proteins at the air–water interface exhibit a very slow development during which the surface (excess) shear viscosity deduced from a Newtonian surface model increases slightly over a period of a day and a half. Then, there is a very rapid increase in the surface shear viscosity to effectively unbounded levels as the interface becomes immobilized. Atomic force microscopy shows that fibrils appear at the interface after it becomes immobilized. Fibrillization in the bulk does not occur until much later. This has been verified by concurrent atomic force microscopy and circular dichroism spectroscopy of samples from the bulk. The immobilized interface has zero in-plane shear rate, however due to the bulk flow, there is an increase in the strength of the normal component of the shear rate at the interface, implicating this component of shear in the fibrillization process ultimately resulting in a thick weave of fibrils on the interface. Real-time detection of fibrillization *via* interfacial rheology may find utility in other studies of proteins at sheared interfaces.

1 Introduction

A large family of disorders known as proteopathic diseases, which includes Parkinson's disease, cystic fibrosis, cataracts, and a variety of prion diseases, are caused by structural dysfunction of specific types of proteins. These proteins adopt conformations different from their native state that serve as pathogenic nucleates. One example of a pathogenic conformation is the amyloid fibril, which is associated with several disorders including Alzheimer's disease. These amyloid aggregates form from chains of misfolded protein that is rich in β-sheet structures, and grow as a result of native protein coming into contact with the nucleates. Understanding how amyloid fibrils form is complicated, in part, because of the wide variety of factors that can lead to the unfolding of native protein and their assembly into this pathogenic form. Perturbations that accelerate fibrillization observed *in vitro* include high protein concentration, extreme pH, heat, vibration, shear, and the presence of hydrophobic interfaces. Hydrophobic interfaces, either solid or fluid, in particular have been shown to have a strong influence on protein misfolding and aggregation both *in vitro* and *in vivo*.[1,2] In light of the ubiquitous presence of interfaces throughout the body, with various degrees of hydrophobicity and fluidity, there have been many studies that have focused on understanding the role of interfaces in disease manifestation.

Fibrillization of various proteins at different interfaces *in vivo* is known to have significant consequences. Some forms of bacteria take advantage of the amyloid structures formed at interfaces to improve the strength and stability of biofilms, which contribute strongly to disease transmission.[3] Mammalian cell walls, which are composed of phospholipid bilayers and membrane proteins, represents one type of hydrophobic fluid interface where soluble proteins may become perturbed and form fibrils. Proteopathic structures have been found to form at cell walls, and disruption of these interfaces by misfolded proteins is one mechanism for disease progression. In particular, disruption of cell membranes *via* formation of amyloidogenic species at interfaces has been linked to diabetes.[4–6] Human islet protein, which is co-secreted with insulin, has been observed to move into the lipid phase of a cell membrane, resulting in disruption and

[a] *Department of Mechanical, Aerospace and Nuclear Engineering, Rensselaer Polytechnic Institute, Troy, NY 12180-3590, USA. E-mail: hirsaa@rpi.edu*
[b] *Department of Biomedical Engineering, Rensselaer Polytechnic Institute, Troy, NY 12180-3590, USA*
[c] *Department of Chemical and Biological Engineering, Rensselaer Polytechnic Institute, Troy, NY 12180-3590, USA*
[d] *School of Mathematical and Statistical Sciences, Arizona State Univ., Tempe AZ, 85287, USA*

cell death.[7–9] Another example is lysozyme, which can form fibrils at interfaces and has been shown to result in cellular disruption and death.[10]

Under quiescent conditions, bulk fibrillization mechanisms are thought to be entirely distinct from interfacial mechanisms.[11] Fibrillization at interfaces is enthalpically driven (as opposed to entropy-driven diffusion in the bulk), and fibrillization occurs approximately three orders of magnitude faster at interfaces than it does in the bulk.[11,12] In addition, the morphology of fibrils at interfaces differ from those formed in the bulk, exhibiting 2D crystalline order.[13] Key factors that enhance the formation of fibrils at hydrophobic interfaces include increased local concentration of protein monomers at the interface, small-scale interactions that promote unfolding of the native state, and easy end-to-end formation of β-sheet structures due to alignment.[2,11,12,14–16] In the bulk, the protein micellar concentration dictates whether or not nucleation will occur, while fibrillization at the air–water interface is dependent on the rate of monomer adsorption and its interaction ability.[11,17]

While the influence of interfaces on fibrillization are relatively well quantified, less is known about the interactions between interfaces and fluid flow. Fluid flow – in particular shearing motion – is prevalent throughout the body, and any understanding of amyloid formation *in vivo* is incomplete without quantification of the combined influences of interfaces and shear. Here, we investigate how shearing flow at hydrophobic fluid interfaces affects amyloid fibril formation. We study the fibrillization of insulin at the air–water interface and in the bulk using a surface viscometer. We utilize a combination of interfacial rheology and standard proteomic techniques to track the fibrillization at the interface and in the bulk.

2 Experimental methods and materials

Fibrillization of human insulin at room temperature (22 °C) was studied through a combination of interfacial rheology and standard techniques for structural determination, namely, atomic force microscopy (AFM) and circular dichroism, along with spectrophotometry for measurements of native protein concentration. To measure the surface (excess) shear viscosity μ^s (Pa s m, equivalently kg s^{-1}), a highly sensitive instrument, namely the deep-channel surface viscometer, was utilized. A schematic of the deep-channel surface viscometer is presented in Fig. 1. This same surface viscometer was used recently to study flow-induced two-dimensional crystallization of protein at the air–water interface,[18] with the modification that in the present study we use Brewster angle microscopy (BAM) to measure the interfacial velocity.

2.1 Interfacial rheology

The deep-channel surface viscometer, depicted in Fig. 1, consists of stationary concentric cylinders of radii R_i and R_o, along with a floor in constant rotation at angular velocity Ω. The flow in this type of surface viscometer has been extensively studied analytically, experimentally, and computationally.[19–24]

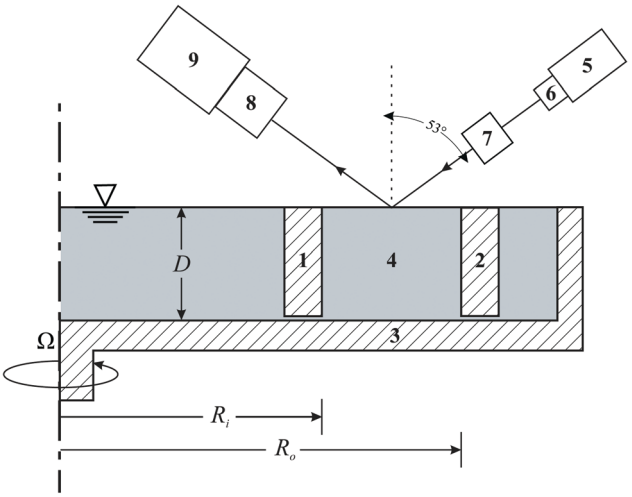

Fig. 1 Schematic of the deep-channel surface viscometer flow geometry along with Brewster angle microscope used in the present study showing the stationary inner cylinder (1), stationary outer cylinder (2), rotating dish (3), region of interest (4), He–Ne laser (5) with a 3× beam expander (6), Glan-laser polarizer (7), zoom lens with a 10× objective (8), and high-speed video camera (9).

The operating principle of the deep-channel surface viscometer is that the more viscous the interface, the slower the interfacial velocity. If the interface has no excess viscosity ($\mu^s = 0$), then the surface velocity has a maximum that is some fraction of the maximum velocity at the floor, which occurs at the corner where the floor meets the outer cylinder. The interfacial velocity can be obtained analytically in the limit of slow floor rotation.[20] On the other hand, at the high rotation rate used in this study, the analytical solution,[19] which assumes linear uni-directional flow, is not valid. The nonlinearity in the Navier–Stokes equations as well as the curvature of the annular channel must be accounted for, and this necessitates a numerical solution. We have detailed elsewhere how to do this.[21,25] The surface shear viscosity, μ^s, in the context of the Newtonian surface model, the so called Boussinesq–Scriven surface model,[20,22] is determined by matching the measured velocity at the interface to the velocity computed for a given μ^s for the geometry and floor rotation rate Ω of the physical experiment.

Hydrodynamics of a given liquid in the deep-channel surface viscometer involves three time scales: (i) the floor rotation time scale, $1/\Omega$, (ii) the viscous diffusion time scale in the bulk, $\rho R_o^2/\mu$, where ρ is the density and μ the dynamic viscosity of the liquid, and (iii) the viscous diffusion time scale at the interface, $\rho R_o/\mu^s$. The ratio of the first two gives the Reynolds number, $\mathrm{Re} = \rho\Omega R_o^2/\mu$, and the ratio of two viscous diffusion times gives the Boussinesq number.

The present deep-channel surface viscometer is constructed of precision-bore glass tubes and an optical window for the floor. The inner radius is R_i = 1.64 cm, and outer radius is R_o = 2.5 cm, and is filled to the rim, with D = 0.85 cm. Extensive experimentation was conducted to determine a suitable rotation rate, Ω. The choice Re = 6000, corresponding to Ω = 9.6 rad s^{-1} was made to be small enough so that the flow would remain

steady and axisymmetric. We have previously established in a similar flow geometry that flow becomes unstable to rotating waves at Re ≈ 12 000, and extensive measurements and simulations have been done at Re = 8000,[21,26] so we selected Re = 6000 to have sufficient margin of stability. Experiments at smaller Re = 600 were conducted, and no significant degree of fibrillization occurred over a week. An added benefit of operating the deep-channel surface viscometer at a high rotation rate is the improved signal-to-noise ratio.[21]

Since this flow system has a large air–water interface, and the experiments ran for about five days, evaporation of water from the protein solution had to be compensated for. DI water was gradually added into the system using a syringe pump. The water was added to the region between the outer stationary cylinder and the rotating dish in order to minimize its impact on the region of interest – between the stationary inner and outer cylinders – where data was gathered. The rate of water addition varied between 0.5 and 0.7 mL h^{-1}, depending on the interfacial conditions of the system. It was determined and verified experimentally that this flow rate ensured that the interface remained flat.

The interfacial velocity measurements were made *via* Brewster angle microscopy. Linearly polarized coherent light of wavelength 633 nm from a He–Ne laser (Melles-Griot, 05-LPL-370-070) was utilized. The 1 mm nominal diameter laser was passed through a 3× beam expander so that the laser footprint on the surface (approximately 3 mm) covers a modest fraction of the full 8.6 mm width of the channel, minimizing the number of scans needed to cover the channel. The expanded beam was then passed through a Glan-laser polarizer so that p-polarized light was incident on the interface. The light reflected off the interface was imaged using a zoom lens (Optem, 70XL) along with a 10× infinity-corrected objective (Mitutoyo, M Plan Apo) and standard TV tube assembly attached to a high-speed video camera (Redlake, HS2-C). The velocity was measured by visually tracking protein clusters at the interface.

2.2 Preparation of insulin solution

Buffer solution of pH 1.6 (0.025 M HCl with 0.1 M NaCl) was made using de-ionized (DI) water with resistivity greater than 18.2 MΩ cm and total carbon content less than 5 ppb (Millipore, simplicity 185-UV, fed with Type-1 DI water). Recombinant human insulin (Sigma Aldrich, 91077C) in powder form was dissolved in the buffer solution. The solution was then pH cycled and twice filtered with a membrane (0.2 μm cellulose acetate syringe filter) following a protocol that has been established to remove impurities and amorphous aggregates for insulin at this pH.[27,28] All the experiments were performed with a final insulin solution concentration of 2 mg mL^{-1}.

2.3 Measurement of soluble insulin concentration

Aliquots of 15 μL protein solution were drawn from the interior of the deep-channel surface viscometer at various times during the operation of the viscometer and were stored in 0.2 mL PCR tubes at 4 °C. These were then centrifuged at 3000*g* for ten minutes to separate any fibrils from the solution. The samples were then analyzed using a spectrophotometer (Nanodrop, UV-vis absorbance along with the ND-1000 software). By measuring the absorbance of the solution at wavelengths 260 nm and 280 nm, the concentration of soluble insulin present at the time of sample extraction was determined. The measurements were made in duplicates to check for reproducibility.

2.4 Atomic force microscopy (AFM)

Samples from both the bulk solution and the interface were analyzed using AFM to study the presence and structure of amyloid fibrils at the interface and in the bulk. For preparation of samples from the bulk, aliquots of 30 μL were drawn and deposited onto 1 cm mica discs (Ted Pella). The protein was allowed to adsorb onto the mica discs for a period of 20 minutes, after which the solution was gently rinsed with DI water and the discs were allowed to air dry.

A modified Langmuir–Schaefer technique was used to liftoff the protein from the interface. A mica disc was gradually lowered until it touched the interface and was then immediately lifted. The mica disc was subsequently inverted and rinsed off using the same procedure as followed for preparing samples from the bulk. An atomic force microscope (Asylum, MFP3D) was used in tapping mode utilizing cantilever tips (Asylum, OLY.AC 240 TS) with a spring constant of 2 at a frequency of 70 kHz.

2.5 Circular dichroism (CD) spectroscopy

Information on the relative amounts of secondary structures present in the bulk protein solution, specifically α-helices and β-sheets, at various times were obtained using CD measurements made with a CD spectrometer (Jasco, 815). Aliquots of 25 μL were removed from the bulk solution and stored in 0.2 mL PCR tubes at 4 °C. Later, the solution was diluted to a concentration of 0.1875 mg mL^{-1} and analyzed in the wavelength range of 190 nm to 260 nm. The CD curves were then averaged based on 4 runs. From the shape of the spectral curves obtained and the location of peaks at specific wavelengths characteristic to the each secondary structure of proteins, the dominant structures present in the protein solution were deduced.

3 Results

The experiments begin by gently filling the thoroughly-cleaned channel with the prepared human insulin solution at room temperature. A small sample from the bulk is taken to establish the initial concentration of the native (monomeric) protein, C_0, then the channel floor is set to a constant rotation. In the absence of surface active material in the system, the flow in this channel would reach steady state in just over one minute.† Adsorption of protein onto the interface changes the viscosity of the interface, and this in turn changes the flow field throughout the channel. Protein interactions at the air–water interface take

† The system reaches hydrodynamic equilibrium within a viscous time, $\rho D^2/\mu \approx$ 75 s. Note that the dynamic viscosity and density of the protein solution is within 1% of water at the same temperature, $\mu/\rho = 0.0096$ cm^2 s^{-1}, and does not change noticeably until fibrillization in the bulk has progressed significantly.[29]

place on a very long time scale and the flow responds to this slowly-changing interfacial condition effectively instantaneously, allowing for the use of a quasi-static approximation for the hydrodynamics.

Measurements of the native protein concentration relative to the initial value, C/C_0, taken at various times made for two separate experiments are presented in Fig. 2. The figure shows that the native protein concentration gradually decreases by about 10% over the first two and half days (60 h). At approximately 75 h the concentration begins to decrease rapidly; this is generally interpreted as marking the end of the nucleation stage and the start of the fibril elongation stage in the bulk.[30] Fig. 2 also shows that it takes about 120 h for the native protein to be fully depleted. This is generally taken to delineate the completion of the fibrillization process. The loss of soluble protein concentration with time has a sigmoidal shape that is often reported in studies of fibrillization kinetics.[1,30,31] Two control experiments done in the same apparatus but under quiescent conditions (Re = 0), also presented in Fig. 2, show that at 120 h native protein concentration in the bulk decreases by less than 3% from its initial value. This is consistent with protein adsorption to the interface. AFM images of protein lifted off the interface in the quiescent case, presented in Fig. 3, show no fibrils are formed in the time that it took the shearing case (Re = 6000) to completely fibrillize.

For the flowing case, Fig. 2 indicates that prior to about t = 70 h the native protein concentration in the bulk had not yet begun its rapid rate of decrease, so one would expect that fibrillization has not begun at that time.[30] AFM images made of fluid taken from the bulk at t = 70 h, presented in Fig. 4(a), verify that there are indeed no fibrils present in the bulk. At t = 120 h the native protein in the bulk had been fully depleted, and the AFM image in Fig. 4(b) shows mature fibrils present in the bulk at this time, as expected.

As an additional indicator of amyloid fibril formation in the bulk, CD measurements were made of liquid samples taken from the bulk and the results are presented in Fig. 5. Fig. 5 shows that the structure of the protein in the bulk, in terms of its ellipsity response, has undergone negligible change in the first 38 hours, indicating that during this time the protein in the bulk

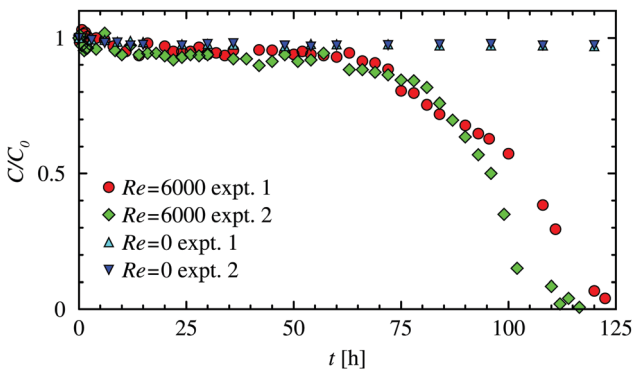

Fig. 2 Temporal evolution of the native protein concentration in the solution relative to its initial value, C/C_0, in the deep-channel surface viscometer with C_0 = 2 mg mL^{-1}. Two sets of experiments are reported, one set with flow at Re = 6000 and the other set quiescent with Re = 0.

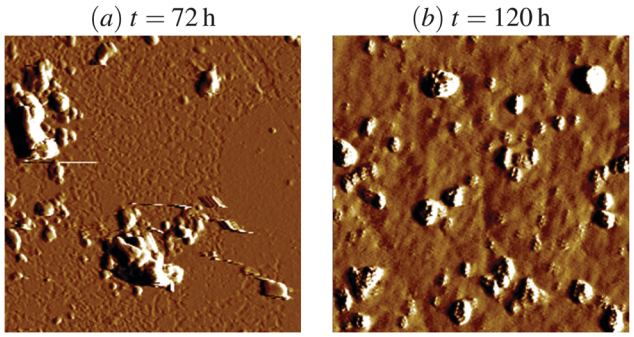

Fig. 3 AFM images of proteins lifted off the interface at times as indicated from a quiescent experiment (Re = 0). Each micrograph corresponds to a region 5 microns × 5 microns.

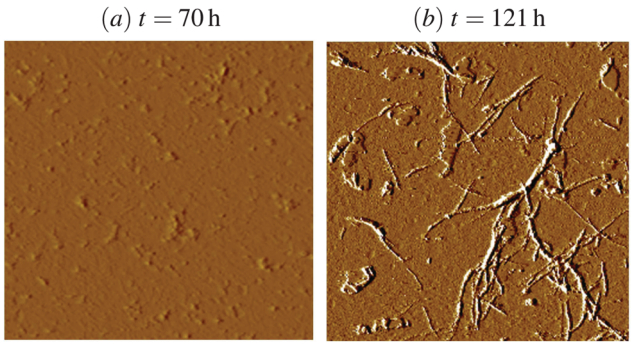

Fig. 4 AFM images of proteins in the bulk at times as indicated from a shearing experiment (Re = 6000). Each micrograph corresponds to a region 5 microns × 5 microns.

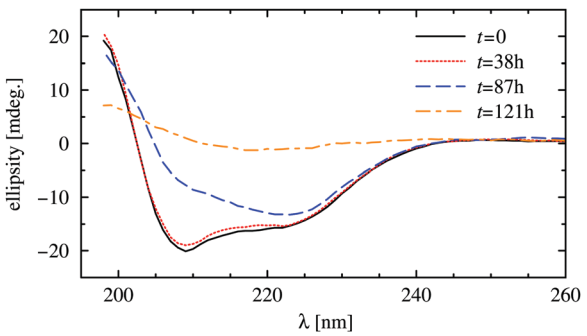

Fig. 5 Circular dichroism plots of bulk samples at times as indicated.

remains mostly in its native state. This is consistent with the protein concentration measurements and AFM images of the bulk which showed that no fibrils were formed prior to t = 70 h. At t = 87 h, Fig. 5 exhibits a noticeable change in the structure of the protein as it nucleates and fibrils begin to grow, consistent with the concentration measurements in Fig. 2 which showed a significant decease in native protein concentration by this time. The relatively flat ellipsity response shown in Fig. 5 at t = 121 h is indicative of the presence of amyloid structures which are rich in β-sheets rather than α-helices.[32] This too is consistent with the measurements of the native protein concentration as well as the AFM images from the bulk solution at this late time.

We now turn our attention to the role of fluid dynamics on the fibrillization process. As mentioned earlier, the flow in the deep-channel surface viscometer would reach equilibrium in about a minute if there were no surface active material present. However, protein is very surface active and its presence on the air–water interface directly alters the surface flow primarily by changing the surface shear viscosity. This in turn alters the fluid flow throughout the channel. In order to determine how the interfacial flow is affected by the presence of protein, we have measured the interfacial velocity in the system. The interfacial velocity profiles measured at various times are presented in Fig. 6(a). Specifically, the measurements are radial profiles of the azimuthal component of velocity at the surface (the only non-zero velocity component at the surface) and are shown as symbols in the figure. The surface shear viscosity at each time is deduced by matching the measured surface velocity profile to computed profiles, shown as solid curves, for various values of μ^s.[21]

Fig. 6(a) shows that after 10 minutes from the start of the experiment (t = 0.17 h), the surface velocity is high and corresponds to a relatively low value of surface shear viscosity (μ^s = 4.8 mg s^{-1}). For the first 26 hours, the change in surface shear viscosity of the interface is small but noticeable, with μ^s increasing to 12 mg s^{-1} over this period. Many studies of protein adsorption have also reported a similar long phase of minor change in interfacial properties.[35–39] This is then followed by a rapid adjustment during which proteins are adsorbed to the interface. Fig. 2 showed that at very early times, on the order of a few hours, long before fibrillization starts in the bulk, some amount of protein (about 5% of C_0) is lost from the bulk, which had adsorbed to the air–water interface. Measurements of the interfacial velocity at the earlier times (up to approximately 26 h), presented in Fig. 6(a), were obtained over a wider portion of the channel than measurements made at the later times. There are two reasons for that, (i) relative changes in velocity with time occurred fast at later times, therefore less time was available to perform a scan by the Brewster angle microscope at any given location on the surface, and (ii) the magnitude of the velocity at late times becomes very small, thus decreasing the signal-to-noise ratio, making velocity measurements away from the channel center less accurate. The wider scan velocity measurements obtained at earlier times generally resemble the shape of the numerical profiles, suggesting that the interfacial response to shear is Newtonian (at least for the earlier times). The lack of reliable velocity measurements away from the center at late times makes it difficult to conclude that the interfacial response is always Newtonian. Shear-thinning response, reported with many interfacial films,[40] may also be occurring here, as discussed below.

Interfacial rheology studies often consider the distribution of the shear in the plane of the interface, $\dot{\gamma} = \partial v/\partial r - v/r$ [s^{-1}]. Here, by selecting the computed velocity at a given μ^s that best fits the measured velocity, we obtain a smooth function that can be differentiated, unlike the discrete velocity data obtained from BAM. The radial profile of $\dot{\gamma}$ corresponding to each of the computed velocity profiles is presented in Fig. 6(b). The $\dot{\gamma}$ profiles show that for the lowest value of surface shear viscosity (μ^s = 4.8 mg s^{-1}), nonlinearity resulting from bulk flow inertia as well as curvature effects make the $\dot{\gamma}$ profile asymmetrical, whereas the asymmetry in the corresponding velocity profile is not as pronounced (see Fig. 6a). The corresponding shear normal to the interface, $v_z = \partial v/\partial z$, determined from the computed bulk flow, is shown in Fig. 6(c) and its significance is discussed below.

Fig. 7 shows a plot of μ^s as a function of time. Note, the velocity profiles for some of the data in Fig. 7, especially near t = 30 h when the velocity becomes very small, were not included in Fig. 6 for clarity. Fig. 7 shows a slow phase of small change in μ^s that is followed by an sudden increase in μ^s within a very short period of time at about $t \gtrsim 27$ h. The interface eventually becomes immobile when the surface shear viscosity attains a high enough value, with μ^s increasing from 24 mg s^{-1} at 28 hours to 240 mg s^{-1} at 30 hours, after which the surface becomes immobile. It is evident that the increase in μ^s is super-exponential in time, and appears to become unbounded at a finite time.

One needs to remain cognizant of the limitations of the Newtonian model used to deduce μ^s at late times. Due to the relatively rapid rate of change in the velocity at late times, the velocity measurements were only made near the center of the channel, as described earlier. This is unlike the early times, when relatively large spans of the channel were measured and

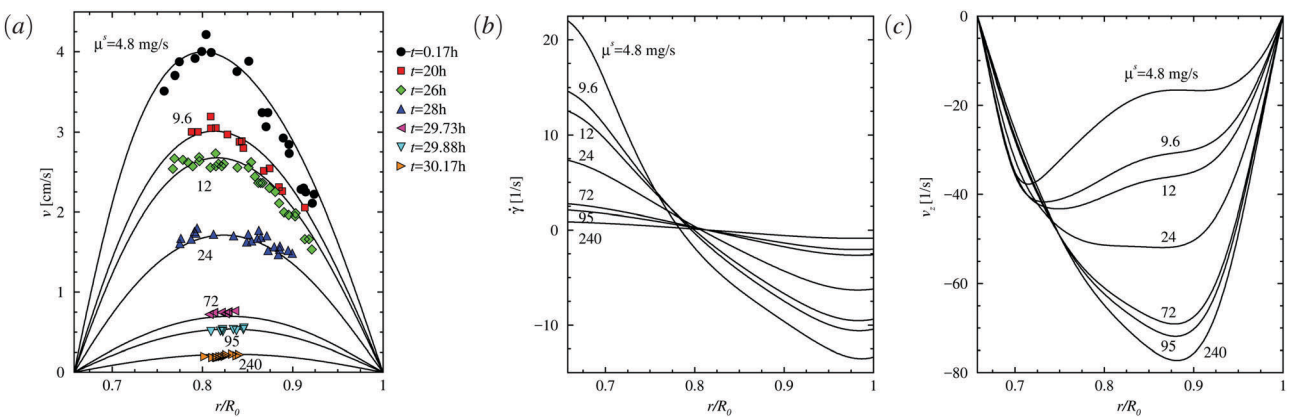

Fig. 6 Radial profiles of (a) the surface azimuthal velocity v [cm s^{-1}] at times as indicated for Ω = 9.6 rad s^{-1} and C_0 = 2 mg mL^{-1} (symbols; experimental) and (lines) numerical profiles at μ^s as indicated, (b) the shear rates $\dot{\gamma}$ [s^{-1}] in the plane of the interface, and (c) the shear rates v_z [s^{-1}] normal to the interface.

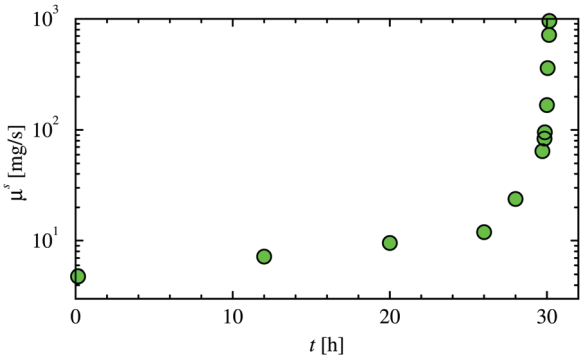

Fig. 7 Temporal evolution of surface shear viscosity, μ^s for Ω = 9.6 rad s^{-1} and C_0 = 2 mg mL^{-1}.

the velocity profiles were found to resemble the shape predicted for a Newtonian interface. It is possible that at the later times, even when the AFM images do not show the presence of fibrils at the interface, the proteins at the interface may have changed confirmation in such a way that the interfacial response to shear is no longer Newtonian, and the μ^s determined by matching measured and computed interfacial velocity profiles using the Boussinesq–Scriven surface model is only an effective, rather than intrinsic, surface shear viscosity that may be dependant on, for example, the local shear rate.[34] This however, is probably only likely to be the case at times $t \gtrsim 26$ h since at earlier times when the velocity profile across most of the channel could be measured matches well with the Newtonian predictions for a given μ^s, indicating that at those times μ^s is quasi-statically independant of the shear rate.

The surface velocity measurements and the inferred surface shear viscosity indicate that the interface has changed radically after about 30 hours. To investigate this, AFM images of protein lifted off the air–water interface at various times were produced. Fig. 8(a) shows one such AFM image, taken at t = 26 h, indicating that there are no fibrils on the interface. The interface at this time appears to have numerous protein structures, presumably oligomers. These oligomeric structures exhibit long-range interactions, as evidenced by the modest value of surface shear viscosity, μ^s = 12 mg s^{-1}, at this time. Fig. 8(b) shows that fibrillization at the interface has already occurred by t = 33 h, which is much earlier than when mature fibrils appear in the bulk (120 h). This is consistent with reports that amyloid fibrils form at the interface earlier than in the bulk in quiescent systems.[2] However, the evolution of the intricately-woven amyloid fibril film at the air–water interface depicted in our AFM images, with the film becoming more densely packed with time, has not been reported previously.

The large difference in time scales between fibrillization in the bulk *versus* fibrillization at the interface is now addressed in terms of the hydrodynamics of the system. At t = 33 h there are no fibrils present in the bulk, and the viscosity in the bulk is unchanged until after t = 75 h. Also, by t = 33 h the interface is completely immobilized so that the interfacial velocity is identically zero and is no longer affected by any further changes in the rheological properties of the interface. Hence, from t = 33 h onwards, the hydrodynamics of the system is at a steady state. At this stage the flow is identical to that in the deep-channel surface viscometer, but with a stationary solid lid (see Fig. 3 of Hirsa *et al.*[21]). This steady flow has a thin but intense boundary layer with large shear stress at the immobilized interface. An intricate mat of interwoven fibrils grows at the interface in this steady flow field over the next three to four days, as indicated by the rest of the AFM images in Fig. 8.

After $t \approx 30$ h, the interface has become immobile, *i.e.* $v \to 0$ at the interface, and hence the shear in the plane of the interface $\dot{\gamma} \to 0$. It is after this time that fibrils begin to be detectable at the interface. This could suggest that fibrillization occurs when the interface is no longer sheared, but this would be a mis-interpretation of what is happening. While the shear in the plane of the interface vanishes, the immobilized interface acts just like a stationary no-slip wall on which an Ekman-like boundary layer develops imparting a normal shear stress at the interface. Fig. 6(c) shows the radial profiles of the normal shear rate at the interface, $v_z = \partial v/\partial z$, at the corresponding μ^s values in Fig. 6(a) and (b). Note that v_z is the forcing term in the tangential stress balance that viscously couples the interfacial and bulk flows.[25,33,34] Although there is uncertainty in the distribution of shear in the plane of the interface at late times, since velocity data is only available near the center, as $t \to \sim 30$ h and the interface becomes immobile, the computed shear distribution in the normal direction is accurate since there are no fibrils in the bulk fluid and it remains Newtonian.

4 Discussion and conclusions

The influence of flow on the fibrillization of insulin at room temperature was studied in a deep-channel surface viscometer. The initial start-up transient in this flow is about a minute.

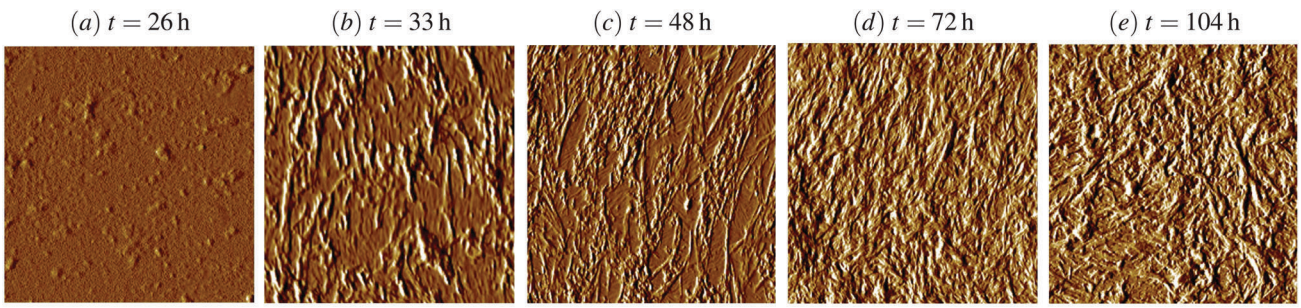

Fig. 8 AFM images of fibrils lifted off the interface at times as indicated. Each micrograph corresponds to a region 5 microns × 5 microns.

The air–water interface has fibrils on it by about 30 hours after starting the flow, but no sign of fibrillization is detected in the bulk until about two days later. During this time the amount of native protein in solution has only reduced by about 10% from its initial concentration. The interface is fully covered by fibrils by about day two, and then the fibril layer thickens with time. Until fibrils appear on the interface, the interfacial flow is slowly diminishing and the surface shear viscosity slowly increases. Then at about 30 hours after the start-up, coinciding with the appearance of the fibrils on the interface, the interface is completely immobilized and the surface shear viscosity has increased by two orders of magnitude. Hence demonstrating for this protein system that surface shear viscosity is a sensitive probe for detecting the onset of fibrillization at the interface.

Although the shear in the plane of the interface vanishes at this point, the fibril-immobilized interface acts as a stationary no-slip boundary, and results in the development of an end-wall boundary layer which has very strong shear normal to the interface. It appears that the shear stress associated with this boundary layer that drives the observed rapid growth of the fibril weave at the interface. As this fibril fabric gets thicker, the shear stress from the boundary layer may be shearing off some fibrils or fragments into the interior flow and thus enhancing fibrillization in the bulk, which took a total of five days to complete.

The interface itself does not need to be shearing or for that matter even flowing, but simply some fibrils on the interface together with relatively slow shearing flow in the bulk can lead to a thick weave of fibrils at the interface within a few days, compared to over a year with no flow.[41] This can have important implications *in vivo*, where interfaces may not be moving, but there is shear flow in their vicinity, and this may play a role in the fibrillization process.

Finally, it should be noted that the fact that the interface becomes immobile after about 30 hours is clearly indicative of a non-Newtonian interfacial response long before any fibrils have formed in the bulk. Refined studies to uncover the relationship between interfacial rheology and fibril formation require more sophisticated models of the interface beyond the single parameter Boussinesq–Scriven model. Recent developments in non-Newtonian interfacial modeling include a single-phase model for shear-thinning interfaces.[34] Another model which may have utility if the interface is covered by untangled fibrils treats them as ellipsoidal colloids confined to the interface.[42] Verification and validation of model results will require significant improvements in the experiments. The Brewster angle microscope utilized here for velocimtery is advantageous due to its non-invasive nature, but it lacks the resolving power and the contrast to see individual fibrils. On the other hand, AFM performed on films lifted off the interface has excellent resolution, but is intrusive in the extreme. Confocal fluorescent microscopy using ThT tag, for example, should provide sufficient spatial resolution, but it will be a challenge to obtain sufficient temporal resolution to parse the interfacial hydrodynamic interactions involved, especially at the time that the interface becomes immobile.

Acknowledgements

This work was supported by NASA grant NNX13AQ22G.

References

1 J. Pronchik, X. He, J. T. Giurleo and D. S. Talaga, *J. Am. Chem. Soc.*, 2010, **132**, 9797–9803.
2 L. Jean, C. F. Lee and D. J. Vaux, *Biophys. J.*, 2012, **102**, 1154–1162.
3 C. Wu, J. Y. Lim, G. G. Fuller and L. Cegelski, *Biophys. J.*, 2012, **103**, 464–471.
4 J. Janson, R. H. Ashley, D. Harrison, S. McIntyre and P. C. Butler, *Diabetes*, 1999, **48**, 491–498.
5 M. Anguiano, R. J. Nowak and P. T. Lansbury, *Biochemistry*, 2002, **41**, 11338–11343.
6 J. R. Brender, U. H. N. Dürr, D. Heyl, M. B. Budarapu and A. Ramamoorthy, *Biochim. Biophys. Acta*, 2007, **1768**, 2026–2029.
7 M. F. M. Engel, *Chem. Phys. Lipids*, 2009, **160**, 1–10.
8 R. Friedman, R. Pellarin and A. Caflisch, *J. Mol. Biol.*, 2009, **387**, 407–415.
9 D. Xiao, L. Fu, J. Lie, V. S. Batista and E. C. Y. Yan, *J. Mol. Biol.*, 2012, **421**, 537–547.
10 A. L. Gharibyan, V. Zamotin, K. Yanamandra, O. S. Moskaleva, B. A. Margulis, I. A. Kostanyan and L. A. Morozova-Roche, *J. Mol. Biol.*, 2007, **365**, 1337–1349.
11 L. Jean, C. F. Lee, C. Lee, M. Shaw and D. J. Vaux, *FASEB J.*, 2010, **24**, 309–317.
12 S. Vembanur, A. J. Patel, S. Sarupria and S. Garde, *J. Phys. Chem. B*, 2013, **117**, 10261–10270.
13 M. Lepère, C. Chevallard, G. Brezesinski, M. Goldmann and P. Guenoun, *Angew. Chem.*, 2009, **121**, 5105–5109.
14 M. Hoernke, J. A. Falenski, C. Schwieger, B. Kokschand and G. Brezesinski, *Langmuir*, 2011, **27**, 14218–14231.
15 S. N. Jamadagni, R. Godawat and S. Garde, *Annu. Rev. Chem. Biomol. Eng.*, 2011, **2**, 147–171.
16 S. Jordens, L. Isa, I. Uzov and R. Mezzenga, *Nat. Commun.*, 2013, **4**, 1917.
17 L. Shen, T. Adachi, D. Vanden Bout and X.-Y. Zhu, *J. Am. Chem. Soc.*, 2012, **134**, 14172–14178.
18 J. E. Young, D. Posada, J. M. Lopez and A. H. Hirsa, *Soft Matter*, 2015, **11**, 3618–3628.
19 R. J. Mannheimer and R. S. Schechter, *J. Colloid Interface Sci.*, 1970, **32**, 195–211.
20 D. A. Edwards, H. Brenner and D. T. Wasan, *Interfacial Transport Processes and Rheology*, Butterworth-Heinemann, Boston, 1991.
21 A. H. Hirsa, J. M. Lopez and R. Miraghaie, *J. Fluid Mech.*, 2002, **470**, 135–149.
22 J. C. Slattery, L. Sagis and E.-S. Oh, *Interfacial Transport Phenomena*, Springer, New York, 2nd edn, 2007.
23 S. R. Derkatch, J. Krägel and R. Miller, *Colloid J.*, 2009, **71**, 1–17.
24 R. Miller, J. K. Ferri, A. Javadi, J. Krägel, N. Mucic and R. Wüstneck, *Colloid Polym. Sci.*, 2010, **288**, 937–950.

25 J. M. Lopez and A. Hirsa, *J. Colloid Interface Sci.*, 2000, **229**, 575–583.
26 A. H. Hirsa, J. M. Lopez and R. Miraghaie, *J. Fluid Mech.*, 2001, **443**, 271–292.
27 D. Posada, P. M. Tessier and A. H. Hirsa, *Biotechnol. Bioeng.*, 2012, **109**, 840–845.
28 S. A. McBride, C. F. Tilger, S. P. Sanford, P. M. Tessier and A. H. Hirsa, *J. Phys. Chem. B*, 2015, **119**, 10426–10433.
29 S. A. McBride, S. P. Sanford, J. M. Lopez and A. H. Hirsa, *Soft Matter*, 2016, **12**, 3461–3467.
30 J. D. Harper and P. T. Lansbury Jr., *Annu. Rev. Biochem.*, 1997, **66**, 385–407.
31 L. Nielsen, R. Khurana, A. Coats, S. Frokjaer, J. Brange, S. Vyas, V. N. Uversky and A. L. Fink, *Biochemistry*, 2001, **40**, 6036–6046.
32 L. Whitmore and B. A. Wallace, *Biopolymers*, 2008, **89**, 392–400.
33 J. M. Lopez and A. Hirsa, *J. Colloid Interface Sci.*, 1998, **206**, 231–239.
34 P. T. Underhill, A. H. Hirsa and J. M. Lopez, *J. Fluid Mech.*, 2017, **814**, 5–23.
35 C. Ybert and J.-M. Di Meglio, *Langmuir*, 1998, **14**, 471–475.
36 R. Miller, V. B. Fainerman, J. Kragel and G. Loglio, *Curr. Opin. Colloid Interface Sci.*, 1997, **2**, 578–583.
37 L. G. Cascão Pereira, O. Theodoly, H. W. Blanch and C. J. Radke, *Langmuir*, 2003, **19**, 2349–2356.
38 S. Mollmann, J. Bukrinsky, S. Frokjaer and U. Elofsson, *J. Colloid Interface Sci.*, 2005, **286**, 28–35.
39 B. C. Tripp, J. J. Magda and J. D. Andrade, *J. Colloid Interface Sci.*, 1995, **173**, 16–27.
40 A. Raghunandan, J. M. Lopez and A. H. Hirsa, *J. Fluid Mech.*, 2015, **785**, 283–300.
41 D. Posada, *Amyloid fibril formation in solution and at interfaces in shearing flows*, PhD thesis, Rensselaer Polytechnic Institute, Troy NY, 2013.
42 A. M. Luo, L. M. C. Sagis, H. C. Öttinger, C. De Michele and P. Ilg, *Soft Matter*, 2015, **11**, 4383–4395.